HIGHLIGHTING THE INFLUENCE OF ARTIFACT SIGNALS ON THE EQUILIBRIUM STATE OF THE FEEDBACK STRUCTURE

Ludovick Lepauloux[1] and Pascal Scalart[2]

[1]Intel Mobile Communications
2600 route des crêtes - 06560 Sophia Antipolis, France
email: ludovick.lepauloux@intel.com

[2]ENSSAT/University of Rennes, INRIA/IRISA/CAIRN
6 rue de Kérampont - 22305 Lannion, France
email: pascal.scalart@enssat.fr

ABSTRACT

In this paper, we address the problem of the determination of the equilibrium point of the feedback structure initially used for two-channel adaptive noise cancellation in the presence of crosstalk. We concentrate on an important characteristic of an adaptive filter, i.e. the steady-state mean-square error observed once the algorithm has converged. Our approach relies on the analysis of the relationships between the useful signals and their artifacts (distortion, residual noise, crosstalk) at the system outputs. The obtained equilibrium point essentially comes from experimental observations, nevertheless, we propose in the first part a theoretical framework that enables to highlight the links between the different signals in the feedback structure and also used to define the equilibrium point. Then, we give experimental results that show that the equilibrium state is obtained when the energy of the artifacts on the output signals is the same on each channel.

1. INTRODUCTION

Identifying an unknown system has been a central issue in various applications areas such as control, equalization, echo cancellation in commmunication networks and many others. In this work, we focus on a particular type of system, namely the symmetric adaptive filter structure, that has been proposed by different authors to solve noise cancellation problems with signal leakage, also called cross-talked problems or cross-coupled interference problems. We concentrate our analysis on the convergence properties and asymptotic behaviour of the feedback separation structure which is represented in Figure 1 in the two-channel case. Such properties have been first studied in very simple cases. Most of the time, stationary input signals and/or single tap mixing filters (instantaneous mixture) were assumed [1, 2] as a consequence of the mathematical complexity of the required analyses [3, 4]. Indeed, the inherent cross-coupling
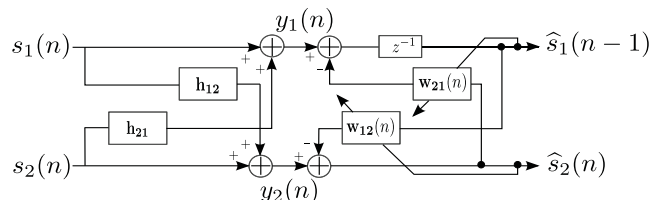

Figure 1: Mixing model (left) and separation structure (right). The introduced delay arbitrarily fixed in the separation structure is justified by implementation considerations.

of this structure introduces an infinite impulse response filter which can lead to potential instability. Thus, the convergence analysis is a critical issue but addressing this problem is more difficult than in classical adaptive FIR filtering because the Hessian matrix associated with the considered structure is time-varying even when the input signals are stationary. Usually, analysis of adaptive filtering algorithms requires simplifying assumptions, such as the small

step-size assumption or the well-known independence assumption between successive regressors, in order to derive expressions that describe the performance of the algorithm. As an example, we can refer to the fixed point theory [5] that is an elegant manner to derive convergence properties of adaptive systems. Although these assumptions are rarely satisfied by real-life data, they render the convergence analysis tractable. Furthermore, when analyzing the feedback structure of Figure 1, we can easily derive an equivalent adaptive identification problem [6] for the adaptive filter $\mathbf{w_{21}}$ (illustrated in Figure 2) where (i) the input sequence $s_2(n)$ and the noise $b(n)$ are mutually dependent, (ii) the noise sequence $b(n)$ is not stationary and (iii) the noise sequence depends on $\mathbf{w_{21}}$. The same analysis holds for the dual filter $\mathbf{w_{12}}$. The above properties are not usual in the context of adaptive filtering and, to our knowledge, no theoretical results have so far been established in such conditions. As a consequence, no useful design guidelines are avalaible to control the convergence of the adaptive feedback system of Figure 1. Nevertheless, some major contributions were produced in
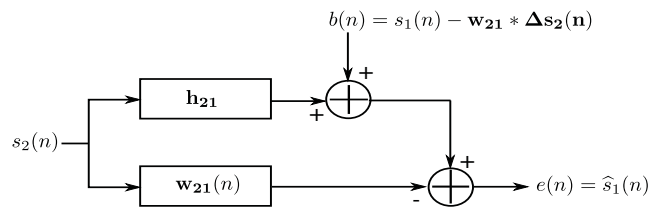

Figure 2: Equivalent adaptive plant identification of $\mathbf{h_{21}}$. On this scheme, $\mathbf{\Delta s_2(n)}$ denotes the vector composed of artifact signals and defined by $\Delta s_2(n) = \widehat{s}_2(n) - s_2(n)$.

the literature. In [7, 8] Charkani and Deville give a complete analysis of the recursive structure for self-adaptive (blind) separation of convolutively mixed signals. On account of ordinary differential equation technique (ODE), equilibrium and stability conditions can be analyzed for a large class of separating functions that are restricted in order to ensure the separating point is an equilibrium state. Indeed, due to the heavy complexity of the obtained mathematical expressions, this study was carried out only around the desired solution ($\mathbf{w_{21}} = \mathbf{h_{21}}$ and $\mathbf{w_{12}} = \mathbf{h_{12}}$) that is assumed to be the equilibrium point corresponding to the separating solutions. In contrast with the common approaches which consist in first defining the adaptive algorithm and then analyzing the behavior of this one according to a given structure, in this paper, we first define analytically useful relations between the different signals. Then, based on energy conservation arguments and under weak assumptions, we define the observed equilibrium point of the separation structure of Figure 1. In that sense, our approach is close to the energy conservation principle developed by Yousef and Sayed [9]. Finally, extensive simulations illustrate the derived results and show the validity of this equilibrium state.

2. PROBLEM STATEMENT

Let us consider the mixing model described in Figure 1. The two observations can be expressed in the Z-domain as:

$$\begin{bmatrix} Y_1(z) \\ Y_2(z) \end{bmatrix} = M(z) \begin{bmatrix} S_1(z) \\ S_2(z) \end{bmatrix}, \quad M(z) = \begin{bmatrix} 1 & H_{12}(z) \\ H_{21}(z) & 1 \end{bmatrix}.$$

Where $M(z)$ denotes the mixing matrix. In order to cancel the existing coupling effect between the observations and to recover the original sources, the separating filters $\mathbf{w_{ij}}$ of the recursive structure shown in the same figure (right side) just have to 'mimic' the filter $\mathbf{h_{ij}}$ of the mixing model, i.e. to converge towards them. Then, inversion of $M(z)$ is actually performed by the recurrent connection. This is the main advantage of the feedback structure in contrast with the feedforward one that needs to estimate the inverse of the mixing matrix $M(z)$.

3. EQUILIBRIUM STATE

In the following, uppercase symbols in boldface font denote matrix quantity whereas lowercase symbols in boldface font indicate a vector quantity. Normal font is used for scalar quantity. The *diag* operator denotes diagonal elements of matrix and $*$ the convolution operator. As stated in Figure 1, $\{s_1, s_2\}$ and $\{y_1, y_2\}$ are respectively the source and the observation signals. We use $\{\widehat{s_1}, \widehat{s_2}\}$ to represent the estimated signals. The following assumptions are used throughout the paper.

- **Assumption A1**. The filter coefficients are slowly varying in time.
- **Assumption A2**. To ensure stability, we impose that $\mathbf{h_{12}}$ is strictly causal.
- **Assumption A3**. The equilibrium state of the feedback structure is obtained when the energy of the artifacts on the output signal is equal on each channel.
- **Assumption A4**. The source signals s_1 and s_2 are assumed to be stationary random variables with zero mean and variance $\sigma_{s_1}^2$ and $\sigma_{s_2}^2$ respectively.

3.1 Artifact analysis on each estimated signal

According to the mixing and separation models, the artifact signals $\Delta s_1(n) = \widehat{s}_1(n) - s_1(n)$ on $s_1(n)$ can be formulated as

$$\Delta s_1(n) = y_1(n) - \mathbf{w_{21}}^T(n)\widehat{\mathbf{s}}_2(n) - s_1(n)$$
$$= \mathbf{h_{21}}^T \mathbf{s_2}(n) - \mathbf{w_{21}}^T(n)\mathbf{y_2}(n) +$$
$$\mathbf{w_{21}}^T(n) diag\left\{\mathbf{W_{12}}^T(n)\widehat{\mathbf{S}}_1(n-1)\right\} \tag{1}$$

with

$$\mathbf{h_{21}} = [h_{21}^0 \ h_{21}^1 \ldots h_{21}^{L-1}]^T,$$

$$\mathbf{w_{21}}(n) = [w_{21}^0(n) \ w_{21}^1(n) \ldots w_{21}^{L-1}(n)]^T,$$

$$\mathbf{y_2}(n) = [y_2(n) \ y_2(n-1) \ldots y_2(n-L+1)]^T,$$

$$\mathbf{s_2}(n) = [s_2(n) \ s_2(n-1) \ldots s_2(n-L+1)]^T,$$

$$\widehat{\mathbf{s}}_2(n) = [\widehat{s_2}(n) \ \widehat{s_2}(n-1) \ldots \widehat{s_2}(n-L+1)]^T,$$

$$\widehat{\mathbf{S}}_1(n-1) = [\widehat{\mathbf{s}}_1(n-1) \ \widehat{\mathbf{s}}_1(n-2) \ldots \widehat{\mathbf{s}}_1(n-L)],$$

$$\mathbf{W_{12}}(n) = [\mathbf{w_{12}}(n) \ \mathbf{w_{12}}(n-1) \ldots \mathbf{w_{12}}(n-L+1)].$$

Assuming that the filter coefficients are slowly time varying [3] (**A1**), i.e. $\mathbf{w_{12}}(n-j) = \mathbf{w_{12}}(n) \quad \forall \ j = 0, \ldots, L-1$, which is equivalent to fix a low step-size (asymptotic behaviour) and noting

that $\mathbf{y_2}(n) = \mathbf{s_2}(n) + \mathbf{S_1}^T(n)\mathbf{h_{12}}$, relation (1) could be reformulated as

$$\Delta s_1(n) = \Delta\mathbf{h_{21}}^T(n)\mathbf{s_2}(n) -$$
$$\mathbf{w_{21}}^T(n)\left[\mathbf{S_1}^T(n)\mathbf{h_{12}} - \widehat{\mathbf{S}}_1^T(n-1)\mathbf{w_{12}}(n)\right]. \tag{2}$$

Where $\Delta\mathbf{h_{21}}(n) = \mathbf{h_{21}} - \mathbf{w_{21}}(n)$ is the weight deviation vector. Let us introduce the matrix

$$\Delta\mathbf{S_1}(n) = \mathbf{S_1}(n) - \widehat{\mathbf{S}}_1(n), \tag{3}$$

and causality constraint (**A2**) on $\mathbf{h_{12}}$ such that $h_{12}(0) = 0$, the expression in the bracket reduces, and (2) yields to

$$\Delta s_1(n) = \Delta\mathbf{h_{21}}^T(n)\mathbf{s_2}(n) -$$
$$\mathbf{w_{21}}^T(n)\left[\widetilde{\mathbf{S}}_1(n-1)\Delta\widetilde{\mathbf{h}}_{12}(n) + \Delta\mathbf{S_1}^T(n-1)\mathbf{w_{12}}(n)\right] \tag{4}$$

where $\widetilde{\mathbf{S}}_1(n-1)$ is a truncated version of $\mathbf{S_1}(n-1)$ of size $L \times (L-1)$. Similarly, $\widetilde{\mathbf{h}}_{12} = \mathbf{h_{12}}(i) \mid_{i=1,\ldots,L-1}$ and $\widetilde{\mathbf{w}}_{12} = \mathbf{w_{12}}(i) \mid_{i=0,\ldots,L-2}$. Similar manipulations can be applied to the artifact signals in second estimated signal $\widehat{s}_2(n)$ leading to

$$\Delta s_2(n) = \Delta\widetilde{\mathbf{h}}_{12}^T(n)\widetilde{\mathbf{s}}_1(n-1) -$$
$$\mathbf{w_{12}}^T(n)\mathbf{S_2}^T(n-1)\Delta\mathbf{h_{21}}(n-1) -$$
$$\mathbf{w_{12}}^T(n)\Delta\mathbf{S_2}^T(n-1)\mathbf{w_{21}}(n-1). \tag{5}$$

Equations (4) and (5) define the artifact signals on the outputs and associated with the feedback structure. The global network corresponding to these two relations is shown in Figure 3. Based on this network, the equilibrium point will be discussed in the next paragraph.

3.2 Conservation of the artifacts energy at each output

Let us assume that the equilibrium state of the feedback structure given in Figure 1 is obtained when the energy of the artifacts on the output signal is the same on each channel (**A3**), i.e. $E\left[\Delta s_1^2(n)\right] = E\left[\Delta s_2^2(n)\right]$. By considering that the filters are slowly time varying, i.e. $\mathbf{w_{21}}(n) * \mathbf{w_{12}}(n) = \mathbf{w_{12}}(n) * \mathbf{w_{21}}(n-1)$, equal output artifact energy ensure identical correlation properties of the signals present at points A and B (see Figure 3). Although it is not universally correct, we will assume that the previous statement is equivalent to the equality of the power spectral densities given hereafter:

$$\Phi_{AA}(e^{j\omega}) = \sum_{k=-\infty}^{\infty} r_{AA}(k)e^{-jk\omega} = \sum_{k=-\infty}^{\infty} r_{BB}(k)e^{-jk\omega}$$
$$= \Phi_{BB}(e^{j\omega}) \tag{6}$$

where $r_{AA}(k) = E\left[A(n)A(n+k)\right]$ is the correlation function of the signal in point A. Assuming that $s_1(n)$ and $s_2(n)$ are independent, we get from Figure 3:

$$\Phi_{AA}(e^{j\omega}) = \Phi_{S_1S_1}(e^{j\omega})\left|\widetilde{H}_{12}(e^{j\omega}) - \widetilde{W}_{12}(e^{j\omega})\right|^2\left|W_{21}(e^{j\omega})\right|^2$$
$$+ \Phi_{S_2S_2}(e^{j\omega})\left|H_{21}(e^{j\omega}) - W_{21}(e^{j\omega})\right|^2. \tag{7}$$

The same reasoning holds in B with $r_{BB}(k)$. By introducing the misalignment vector, the power spectral densities can be rewritten as

$$\Phi_{AA}(e^{j\omega}) = \Phi_{S_1S_1}(e^{j\omega})\left|\Delta\widetilde{H}_{12}(e^{j\omega})\right|^2\left|W_{21}(e^{j\omega})\right|^2 +$$
$$\Phi_{S_2S_2}(e^{j\omega})\left|\Delta H_{21}(e^{j\omega})\right|^2 \tag{8}$$

$$\Phi_{BB}(e^{j\omega}) = \Phi_{S_2S_2}(e^{j\omega})\left|\Delta H_{21}(e^{j\omega})\right|^2\left|W_{12}(e^{j\omega})\right|^2 +$$
$$\Phi_{S_1S_1}(e^{j\omega})\left|\Delta\widetilde{H}_{12}(e^{j\omega})\right|^2. \tag{9}$$
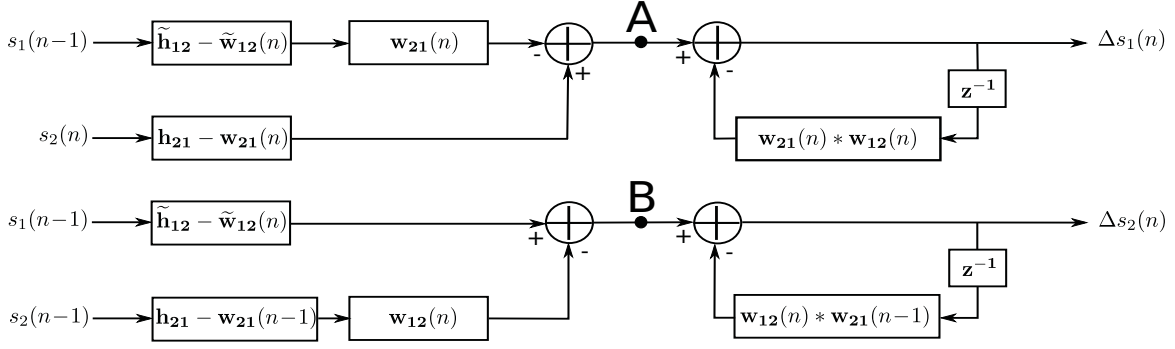
Figure 3: Global network for getting the artifact signals on each channel.

Inserting (8) and (9) into (6), we get the following equilibrium relationship for the feedback structure:

$$\frac{\left|\Delta\widetilde{H}_{12}(e^{j\omega})\right|^2}{\left|\Delta H_{21}(e^{j\omega})\right|^2} = \frac{\Phi_{S_2S_2}(e^{j\omega})}{\Phi_{S_1S_1}(e^{j\omega})} \cdot \frac{\left|W_{12}(e^{j\omega})\right|^2 - 1}{\left|W_{21}(e^{j\omega})\right|^2 - 1}. \quad (10)$$

By exploiting the usual spectral analysis of the time-invariant (stationary) system for some fixed $W_{12}(z)$ and $W_{21}(z)$, the obtained relation is valid whatever the coefficients of the separating filters are. And note that the originality of our approach stands in the fact we apply it to artifact signals what has never been done yet.

3.3 Signal to artifact ratio (SAR) analysis

Through the above analysis, the signal to artifact ratio on each channel could be easily defined as follow:

$$
\begin{aligned}
SAR_1(e^{j\omega}) &= \frac{\Phi_{S_1S_1}(e^{j\omega})}{\Phi_{\Delta S_1 \Delta S_1}(e^{j\omega})} \\
&= \Phi_{S_1S_1}(e^{j\omega})\frac{\left|1 - W_{12}(e^{j\omega})W_{21}(e^{j\omega})e^{-j\omega}\right|^2}{\Phi_{AA}(e^{j\omega})}
\end{aligned}
\quad (11)
$$

$$
\begin{aligned}
SAR_2(e^{j\omega}) &= \frac{\Phi_{S_2S_2}(e^{j\omega})}{\Phi_{\Delta S_2 \Delta S_2}(e^{j\omega})} \\
&= \Phi_{S_2S_2}(e^{j\omega})\frac{\left|1 - W_{12}(e^{j\omega})W_{21}(e^{j\omega})e^{-j\omega}\right|^2}{\Phi_{BB}(e^{j\omega})}.
\end{aligned}
\quad (12)
$$

Then, according to the stated equality principle expressed in (6), the following important relation holds

$$\frac{SAR_1(e^{j\omega})}{SAR_2(e^{j\omega})} = \frac{\Phi_{S_1S_1}(e^{j\omega})}{\Phi_{S_2S_2}(e^{j\omega})}. \quad (13)$$

This relation describes the behavior of the feedback structure and is valid whatever the nature of the signals sources are and whatever the value of impulse responses of identification filters $\mathbf{w_{12}}(n)$ and $\mathbf{w_{21}}(n)$ are. Note that if the two sources $s_1(n)$ and $s_2(n)$ correspond to white noise, the ratio given by (13) is equal to the average power ratio $\sigma_{s_1}^2/\sigma_{s_2}^2$ between the source signals.

4. EXPERIMENTAL RESULTS

4.1 Convergence: transient and steady-state analysis

In this section we present simulation results illustrating the validity of the asymptotic analysis presented previously. In these experiments, the signal $s_2(n)$ corresponds to a zero mean white Gaussian

noise with $\Phi_{S_2S_2}(e^{j\omega}) = \sigma_{s_2}^2$. The input signal $s_1(n)$ is a Gaussian first order autoregressive process (AR) with variance $\sigma_{s_1}^2$ and with pole $\alpha \in [0,1[$. To adapt the adaptive filters $\mathbf{w_{12}}(n)$ and $\mathbf{w_{21}}(n)$, we choose the symmetric adaptive decorrelation algorithm, [1]:

$$\mathbf{w_{ji}}(n+1) = \mathbf{w_{ji}}(n) + \mu \widehat{s_i}(n)\widehat{\mathbf{s_j}}(n) \quad \forall\, i \ne j \in 1,2 \quad (14)$$

where $\widehat{\mathbf{s_j}}(n) = [\widehat{s_j}(n)\ldots\widehat{s_j}(n-L+1)]^T$ denotes the vector of the last L output samples of the separating filters. We assume perfect modelisation with separating filters having the same length as the mixing ones. In the experiments, coupling filters of order $L = 20$ are used and the separating filters are adapted from the relationship (14) with a low step-size, $\mu = 10^{-4}$.

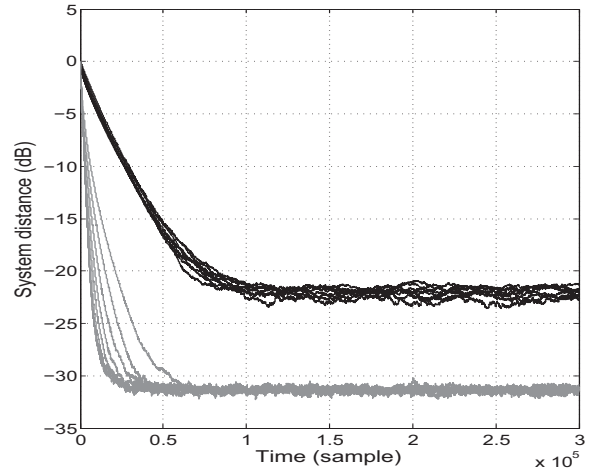Figure 4 shows, for a signal to noise ratio of 10 dB and for colored

Figure 4: Convergence of the system distance $\|\Delta\mathbf{h_{12}}(n)\|^2 / \|\mathbf{h_{12}(n)}\|^2$ (grey) and $\|\Delta\mathbf{h_{21}}(n)\|^2 / \|\mathbf{h_{21}(n)}\|^2$ (black) for different values of the pole $\alpha = 0, 0.1, 0.2, \cdots, 0.9$.

signal $s_1(n)$, the convergence of the system distance over time of the two filters $\mathbf{w_{12}}(n)$ and $\mathbf{w_{21}}(n)$. We can observe that the behavior of the transient phase is different between the two channels, the fastest convergence being obtained in the most energetic channel.

4.2 Signal to artifact ratio on each channel

We now consider the previously established relations expressing the signal to artifact ratio at the output of each channel of the feedback structure. In this paragraph, we assume that the source signals are the ones described previously. It is possible to compute, at each time instant n, the power spectral densities (8) and (9) by observing

the coefficients of the separating filters at that time instant. Once the power spectral densities $\Phi_{AA}(e^{j\omega})$ and $\Phi_{BB}(e^{j\omega})$ are known, we can then express, from relations (11) and (12), the value of the SAR on each spectral component of both channels. Such curves are displayed in Figure 5 (top) when the source signal $s_1(n)$ is an AR (1) signal with pole $\alpha = 0.8$ and with an average power ratio of $\sigma_{s_1}^2/\sigma_{s_2}^2 = 10$. These curves are obtained by considering mean values $\overline{\mathbf{w}}_{12} = \lim_{n\to\infty} E[\mathbf{w}_{12}(n)]$ and $\overline{\mathbf{w}}_{21} = \lim_{n\to\infty} E[\mathbf{w}_{21}(n)]$, which is equivalent to consider asymptotic behavior of the adaptive filters. The curve in Figure 5 (bottom) corresponds to the evalua-
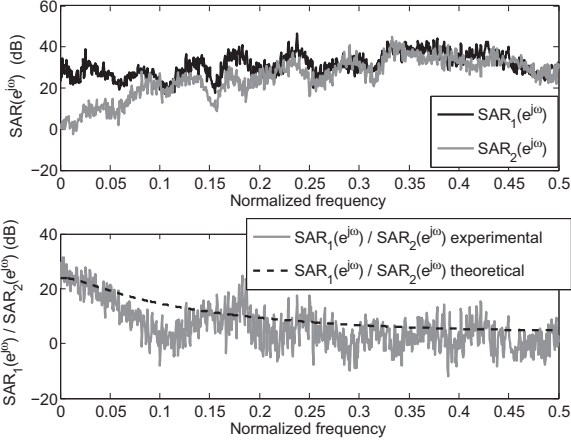

Figure 5: Frequency behavior of $SAR_1(e^{j\omega})$ and $SAR_2(e^{j\omega})$ (top) and $SAR_1(e^{j\omega})/SAR_2(e^{j\omega})$ (bottom).

tion of (13) under the same experimental conditions. In noting that the theoretical power spectral density (PSD) of the AR(1) source is given by:

$$\Phi_{S_1 S_1}(e^{j\omega}) = \sum_k r_{S_1 S_1}(k)e^{-jk\omega} = \frac{(1-\alpha^2)\sigma_{s_1}^2}{1+\alpha^2 - 2\alpha\cos\omega}, \qquad (15)$$

it is possible to also represent on Figure 5 (dashed curve) the theoretical value of this ratio, which is given by

$$\frac{SAR_1(e^{j\omega})}{SAR_2(e^{j\omega})} = \frac{\sigma_{s_1}^2}{\sigma_{s_2}^2} \times \frac{(1-\alpha^2)}{1+\alpha^2 - 2\alpha\cos\omega}. \qquad (16)$$

From this figure, we note the capability of the theoretical relation given by (16) to closely predict the behavior of the experimental curve (we recall here that the PSD given by (15) obtained through AR parametric modeling is able to model spectral envelope maxima). Let us define the frequency average SAR noted SAR^{fb}, obtained by integrating $SAR_i(e^{j\omega})$ with $i = \{1,2\}$ over the whole spectral domain.

$$SAR_i^{fb} = \int_{-\pi}^{\pi} SAR_i(e^{j\omega})d\omega$$

Consequently and according to (13), the ratio of the full-band SAR should be equal to the average power ratio of the sources. To compute these full-band SAR, we do not use the mean values of $\mathbf{w}_{12}$ and $\mathbf{w}_{21}$. We compute these full-band SAR directly by using the experimental signals $E[(s_1 - \hat{s}_1)^2]$, $E[(s_2 - \hat{s}_2)^2]$, $E[s_1^2]$ and $E[s_2^2]$, that is to say all along the convergence of the filter without limiting to the asymptotic behavior with the mean value of the filters. Consequently, we observe the validity of the obtained relations also during the convergence of the filters. Under the same experimental conditions as above, we can see that the experimental results in Figure 6 (bottom) are consistent with the theoretical analysis expressed in (13). In fact, even during the initial convergence,
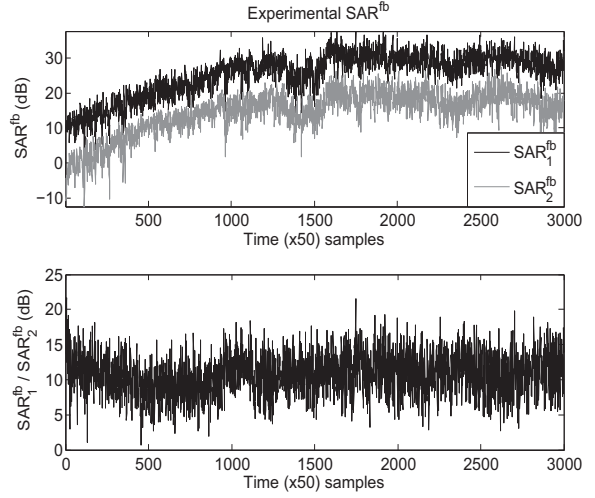

Figure 6: Time evolution of SAR_1^{fb} and SAR_2^{fb} (top), and SAR_1^{fb}/SAR_2^{fb} (bottom).

the difference (in dB) between each SAR^{fb} of the two channels is equal to 10 dB which agrees with $\sigma_{s_1}^2/\sigma_{s_2}^2 = 10$. The accuracy of the theoretical predictions tends to validate the assumption (**A3**) made in the theoretical analysis. Namely, *at each time instant n, the two separating filters of the feedback structure adjust their time-varying impulse responses according to the following rule: the energies of the artifact signals on each output are equal.* To further validate
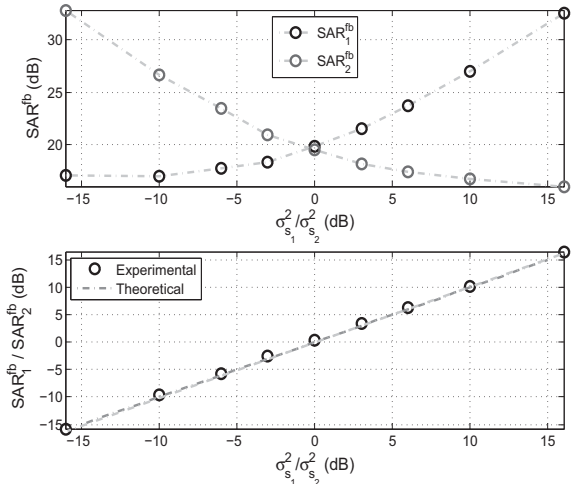

Figure 7: Frequency average SAR^{fb} obtained on channel 1 and 2 when $\alpha = 0$ for different values of $\sigma_{s_1}^2/\sigma_{s_2}^2$.

our theoretical analysis (and therefore the underlying assumptions), we give in Figure 7 and Figure 8 the full-band SAR values obtained during the steady-state convergence phase of the algorithms for different configurations of the input sources power ratio $\sigma_{s_1}^2/\sigma_{s_2}^2$. On Figure 7 the two input signals $s_1(n)$ and $s_2(n)$ correspond to white Gaussian noise process ($\alpha = 0$) and AR(1) signals with pole $\alpha = 0.4$ and $\alpha = 0.7$ in Figure 8. We can see from Figure 7 (bottom) and Figure 8 (right) that, in all considered cases, the ratio between the experimental full-band SAR^{fb} of each channel is equal to $\sigma_{s_1}^2/\sigma_{s_2}^2$, also with colored signals and as predicted by the theoretical analysis. Finally, we test the robustness of our analysis with speech
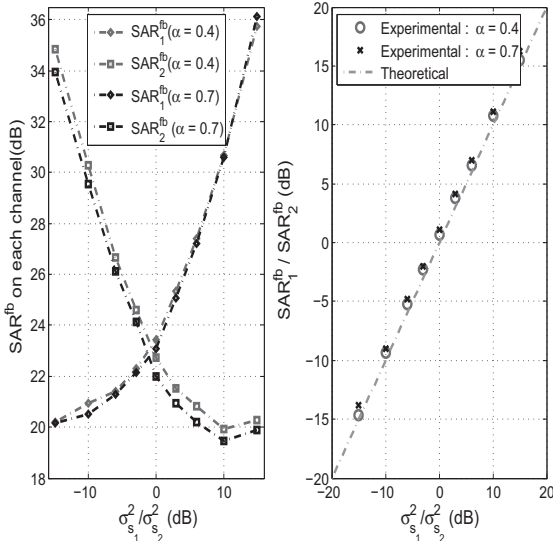
Figure 8: Frequency average SAR (SAR^{fb}) obtained on channel 1 and 2 when $\alpha = 0.4$ and $\alpha = 0.7$ for different values of $\sigma_{s_1}^2/\sigma_{s_2}^2$.

Figure 10: Frequency average SAR (SAR^{fb}) obtained on channel 1 (black) and 2 (grey) with speech sources for different values of $\sigma_{s_1}^2/\sigma_{s_2}^2$.

signals. Consequently, we are no more compliant with assumption (**A4**). The input signal-to-noise ratios are computed using the ITU-T recommendation P.56 speech voltmeter (SV56). The speech signals are recorded from a male and a female speakers and shown in Figure 9. Results are given on Figure 10.

noise cancelling problems or equally for blind source separation. However, nothing enables us to ensure that the observed equilibrium point is unique. A better theoretical description is needed to deal with this point that will be investigated in future work.
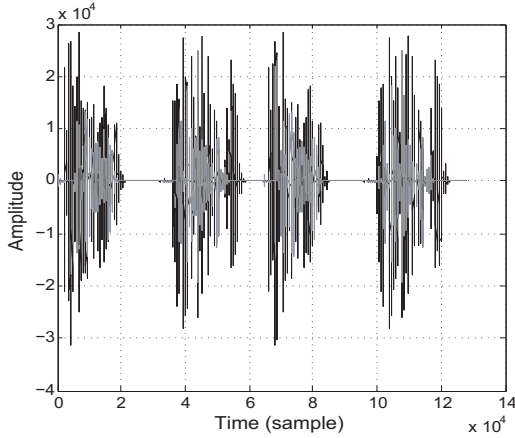
Figure 9: Time-amplitude plot showing signal mixture.

As before with stationary signals, the same behavior is observed. We can see that the evaluated ratio corresponds to the average power ratio of the speech sources across all considered SNRs. Thus, the assumption (**A3**) seems to be consistent even with speech signals.

5. CONCLUSION

In this paper, the intrinsic convergence properties of the two-channel feedback structure have been discussed. Based on the analysis of the relationship between output signals and their artifacts, we have shown that the equilibrium state is obtained when the energy of the artifacts on the output is the same on each channel. Thus, this paper provides new relations for further analyzing the convergence and stability properties of the feedback structure widely used for
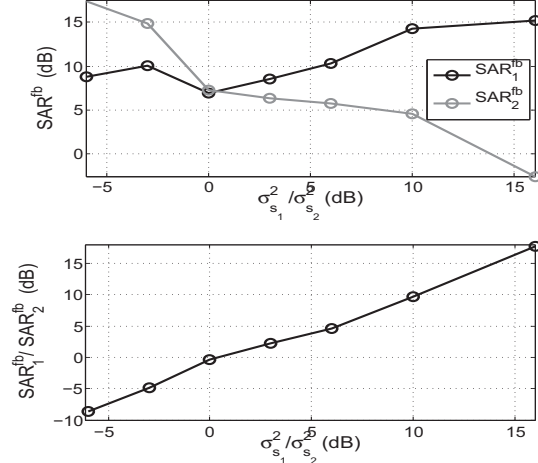
REFERENCES

[1] S. Van Gerven and D. Van Compernolle. Signal separation by symmetric adaptive decorrelation : stability, convergence and uniqueness. *IEEE Trans. on Signal Processing*, 43:1602–1612, 1995.

[2] E. Weinstein, M. Feder, and A. V. Oppenheim. Multi-channel signal separation by decorrelation. *IEEE Trans. Speech and Audio Processing*, 1:405–413, 1993.

[3] L. Lepauloux, P. Scalart, and C. Marro. An efficient low-complexity algorithm for crosstalk-resistant adaptive noise canceller. In *EUSIPCO*, 2009.

[4] G. Mirchandani, R. L. Zinser, Jr., and J. B. Evans. A new adaptive noise cancellation scheme in the presence of crosstalk. *IEEE Trans. on circuits and systems II*, 39:681–694, 1992.

[5] D. Mandic and I. Yamada. Machine learning and signal processing applications of fixed point theory. Tutorial at ICASSP, 2007.

[6] Eweda Eweda. A new approach for analyzing the limiting behavior of the normalized lms algorithm under weak assumptions. *Signal Processing*, 89(11):2143–2151, November 2009.

[7] N. Charkani and Y. Deville. Self-adaptive separation of convolutively mixed signals with a recursive structure. part i: stability analysis and optimization of asymptotic behaviour. *Signal Processing*, 73:225–254, 1999.

[8] N. Charkani and Y. Deville. Self-adaptive separation of convolutively mixed signals with a recursive structure. part ii: theoretical extensions and application to synthetic and real signals. *Signal Processing*, 75:117–140, 1999.

[9] N. R. Yousef and A. H. Sayed. A unified approach to the steady-state and tracking analyses of adaptive filter. *IEEE Trans. on Signal Processing*, 49(2):341–324, February 2001.